A Letters Journal Exploring the Frontiers of Physics

OFFPRINT

High-velocity drag friction in dense granular media

Yuka Takehara, Sachika Fujimoto and Ko Okumura

EPL, **92** (2010) 44003

A Letters Journal Exploring the Frontiers of Physics

November 2010

EPL, **92** (2010) 44003
doi: 10.1209/0295-5075/92/44003

www.epljournal.org

High-velocity drag friction in dense granular media

Yuka Takehara, Sachika Fujimoto and Ko Okumura[a]

Department of Physics, Ochanomizu University - 2-1-1, Otsuka, Bunkyo-ku, Tokyo 112-8610, Japan

received 25 May 2010; accepted in final form 8 November 2010
published online 10 December 2010

PACS 45.70.Mg – Granular flow: mixing, segregation and stratification
PACS 47.57.Gc – Granular flow
PACS 89.75.Da – Systems obeying scaling laws

Abstract – We study drag force acting on an obstacle in granular media, focusing on a high-velocity region where only a few direct studies are available. The granular media are two-dimensional and consist of small-sphere particles. A larger-disk obstacle moves in the medium at different constant speeds. The drag force is found to be proportional to the square of the velocity. We explain the observed relations by developing original scaling arguments and by demonstrating a clear data collapse. As a result, we conclude that the friction we observed is physically different from a hydrodynamic inertial friction, which has been discussed in dilute granular flows and in impact experiments. The high-velocity drag friction observed in this study may be attributed to another mechanism, where the formation of the dynamical force chains plays a crucial role.

Introduction. – Understanding and modeling of granular materials, which can significantly contribute to industries, agriculture and construction [1], are highly nontrivial and a plenty of efforts has been made in many different fields of physical sciences [2–4] including geophysics [5]. An important issue is the drag force exerting on an obstacle in a dense granular medium. Creep motions of an obstacle, related to jamming transitions, have been studied extensively [6,7] where the drag force is found to be independent of [8,9] or logarithmically dependent on [10,11] velocity. Oppositely, extremely high-velocity motions of the order of 1 m/s have been also studied actively in the context of impact experiment where drag force in dense granular media can be constructed *indirectly* (the speed of the obstacle changes during the impact) [12,13]. Contrary to these two extreme velocity ranges, motions of an obstacle in a relatively high-velocity range of the order of a few 100 mm/s have been less studied although the independence from velocity of the drag force is reported *under a strong influence of gravity* [14].

In this paper, we *directly* study a drag force at relatively high velocities ($\sim$ a few 100 mm/s) in dense granular flows. By using a horizontally placed two-dimensional cell, the dynamics is virtually *free from the influence of gravity*. We find a squared velocity dependence of the drag force. This seems at sight similar to the hydrodynamic inertial force discussed in the impact experiments [12,13] or in dilute granular flows [15–17]. However, we conclude that, unlike in the previous observations, the drag force we observed is not a hydrodynamic one and reflects the effect of non-binary collisions. This conclusion is drawn by developing a simple and original scaling argument based on the spirit of the Bagnold theory [18,19] and by demonstrating a good agreement between our theory and experiment.

Experiment. –

Experimental details. To measure the drag force, we fabricated a transparent cell from two acrylic plates of thickness 3 mm, motivated by [20]. These plates are separated in parallel by spacers of thickness 2 mm at the four edges to make a cell of length $L_x = 430$ mm, of width $L_y = 120$ mm and of depth 2 mm (fig. 1(a)). We filled this cell with commercial particles of aluminium oxide and a disk obstacle. The average diameter of the particles $2d$ and the thickness of the obstacle are both slightly smaller than the cell thickness. The disk obstacle is actually a commercial washer of radius R with a hole of radius R_0 at the center. We changed the radius R from 10 to 15 mm with keeping the 2D packing fraction ϕ of smaller particles to a constant value 0.797. Here, ϕ is estimated as $\phi = \pi d^2 N/S$, where N (roughly around 10000) and S are the number of particles and area allowed for particles (*i.e.*, $S = L_x L_y - \pi R^2$), respectively; note that in the present case the 2D granular system consists not of disks but of less voluminous spheres. The alumina balls are

[a] E-mail: okumura@phys.ocha.ac.jp

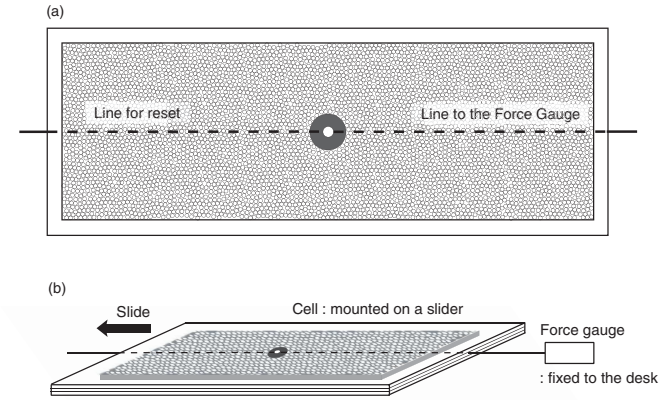

Fig. 1: Experimental setup. (a) Two-dimensional cell made of acrylic plates filled with an obstable (washer) and smaller spheres. (b) The cell mounted on a slider with an obstable inside the cell connected to a force gauge through a non-extensible fishing line. The cell can move in the arrow direction at different constant speeds while the force gauge is fixed to the desk.

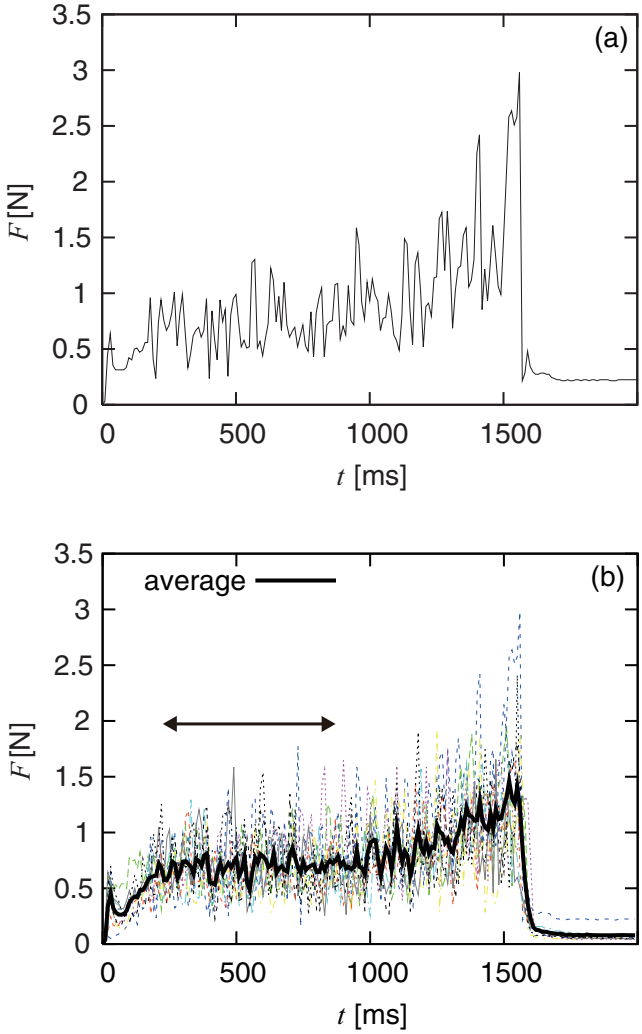

Fig. 2: (Colour on-line) Drag force exerted on an obstable of radius 10 mm as a function of time at moving velocity 200 mm/s. (a) Result obtained from a single-drag experiment. (b) Superposition of the results from 10-drag experiments with the average curve which exibits less fluctuation with a distinct stationary regime (indicated by an arrow) in the middle.

polydispersed; the maximum radius (of randomly selected 100 particles used in the experiments) was 1.13 mm and the minimum 0.93 mm with the mean and polydispersity Δ being 1.05 mm and 0.042, respectively. Here, polydispersity is defined as $\Delta = \sqrt{\langle d^2\rangle - \langle d\rangle^2}/\langle d\rangle$ with $\langle d\rangle$ denoting the average of the radii of the granular particles. We attached the cell on a moving stage of a slider (EZS3D060-K, Oriental Motor) which allows us to slide the cell at different constant speeds; an obstacle is connected to a force gauge (FGP-0.5, NIHON DENSAN SIMPO) via a fishing line (which is almost non-extensible) to monitor drag force exerted on the obstacle (fig. 1(b)); we move the cell on a fixed table with the disk obstacle fixed while we shall discuss the movement of the disk obstacle in the frame fixed to the (moving) cell in the following, if not specified.

Results of drag force measurements. A typical result for the relation between drag force and elapsed time obtained from a single-continuous-drag experiment at a fixed speed is given in fig. 2(a). The force fluctuates tremendously but when such results from 10-drag experiments at the same speed are superposed as in fig. 2(b) the average force-time curve exhibits less fluctuations and a clear stationary region with a well-defined average, except the initial transient region and the final region; in the final region the force increases due to the right edge of the cell.

When we plot the average F thus obtained for a fixed disk radius R as a function of the velocity V, we find unexpectedly smooth curves as in fig. 3, in spite of severe fluctuations in fig. 2. Here and hereafter F denotes the average of drag forces. These non-linear relation between F and V indicate that this medium is non-Newtonian. By plotting this average force F as a function of V^2 in fig. 3(b), we can clearly confirm the relation

$$F = F_0 + \alpha V^2, \tag{1}$$

where F_0 corresponds to the intersect of the straight lines with the vertical axis in fig. 3(b).

Theory. –

Scaling arguments. The law (1) thus established experimentally can be explained as follows. Mimicking the basic idea of Bagnold, we regard the dynamical component of the drag force, $F - F_0$, as change in the momentum of the obstacle per time where the momentum change is caused by collision with smaller particles:

$$F - F_0 = \nu M \Delta V. \tag{2}$$

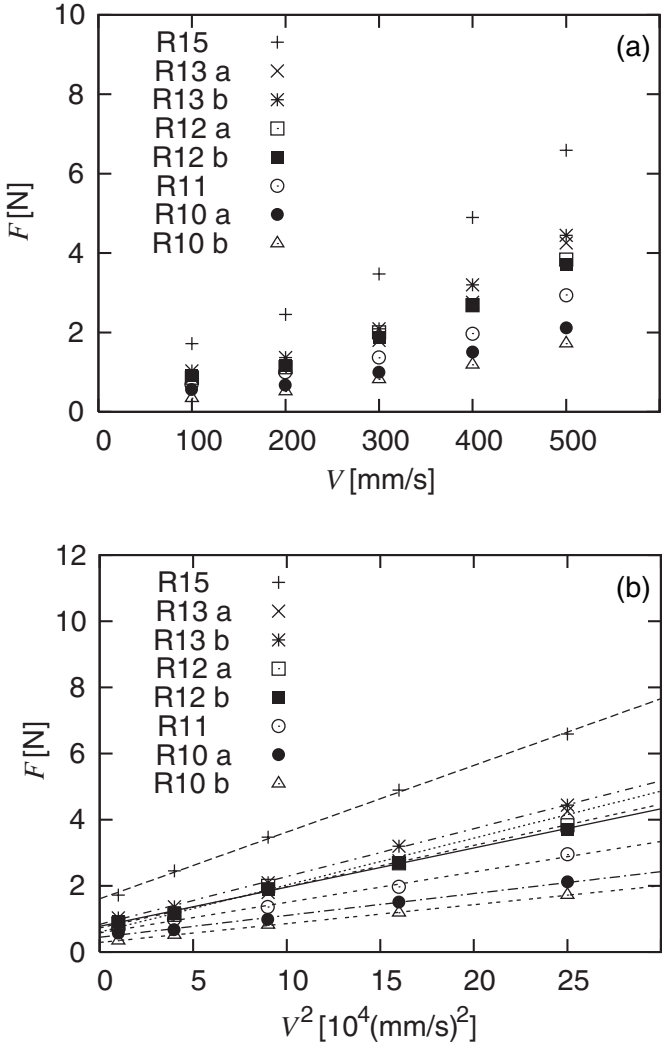

Fig. 3: (a) Plots of the average drag force as a function of moving velocity for different radii of the obstacle ($R = 10$, 11, 12, 13 and 15 mm) where each data point is obtained from ten-drag experiments as in fig. 2(b). Here and hereafter, the notations, R15, R13a, R13b, and so on denote the data for particles of radii $R = 15$ mm and of $R = 13$ mm for two data sets, and so on. (b) Plots of the average drag force as a function of squared velocity using the same data in (a), which establishes eq. (1).

Here, M and ΔV are mass and average velocity change (per one collision) of the obstacle while ν is number of collision per time:

$$M = 2\pi\rho(R^2 - R_0^2)d, \tag{3}$$

$$\nu = 2RV\phi/(\pi d^2), \tag{4}$$

where ρ is the density of the obstacle. Thus, if ΔV scale as V we immediately obtain $F - F_0 \sim V^2$, as expected.

This last point can be justified at the level of scaling law if we consider a linear collision between the obstacle of mass M and another "particle" of mass m with the initial velocities V and v and with the final V' and v'. When the restitution coefficient is e, from the momentum conservation, we obtain

$$\Delta V \equiv V - V', \tag{5}$$

$$= \frac{m(1+e)}{m+M}(V - v). \tag{6}$$

Thus, when $V \gg v$ as we can directly observe in our experiments, ΔV certainly scales as V as desired. Note, however, that, if the mass m were much smaller than the mass M, although the velocity change ΔV would scale as V in eq. (6), the former would become much smaller than the latter; the situation would be similar to a granular Brownian motion [21] and the drag force would be linear in the velocity. Below, we show that the mass m is actually of the same order as the mass M.

Dynamical phase separation: percolated cluster. We now discuss the order of m in the present case, or, size of the "particle" with which the obstacle of mass M collides in a single collision. We could simply identify this particle with a single alumina particle of radius d, which means $m = 4\pi d^3\rho'/3$ with ρ' the density of the smaller particle. However, we insist here that in the present case another consideration is appropriate: each time the obstacle collides with a small particle the particle is connected via force chains to other surrounding particles, and such force chains develop around the obstacle only in a region of size of the obstacle. Thus, though nontrivial, we assume that m scales as M (ρ/ρ' is a constant of the order of unity): at each collision (with the rate ν), the obstacle collides with a transient *percolated cluster* of only available length scale R (and of mass M).

As a matter of fact, if we observe the movement of small particles around the obstacle *in the coordinate fixed to the obstacle*, we clearly notice the particle medium is separated into two domains or phases.

In the first region which is within a distance around R from the obstacle, small particles move incessantly and randomly due to collisions around the obstacle. In this region particles develop dynamically changing force chains to form the percolated cluster.

In the second region which is outside of the first region, small particles homogeneously move at constant velocity (*i.e.* not moving at all in the coordinate fixed to the cell forming static force chains).

The dynamical force chains are cut at the boundary of the two regions or phases (at a distance around R from the obstacle). Only particles within the percolated cluster region join the collision. In other words, the medium is dynamically separated into two phases.

Comparison with the experiment. This nontrivial assumption is strongly supported by our experimental data. When we do assume $m \simeq M$ we have $\Delta V \simeq V$ so that eq. (1) can be cast into the following scaling law with a numerical coefficient k:

$$F/F_0 - 1 = (kV/V_0)^2. \tag{7}$$

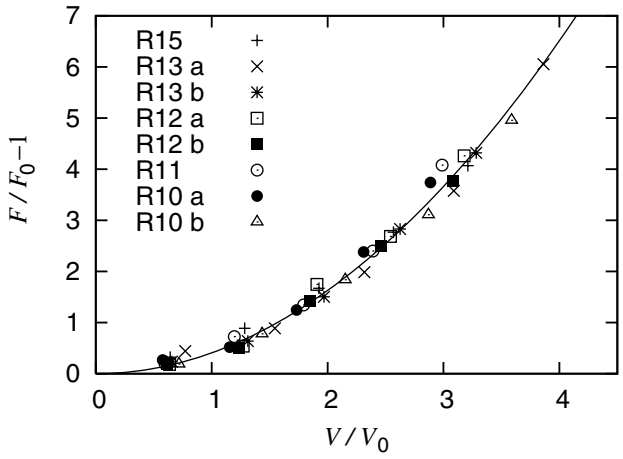

Fig. 4: Rescaled plot of fig. 3(a). All the data in fig. 3(a) collapse onto a master curve as predicted by eq. (7). The curve representing the master curve corresponds to $k = 0.638$.

Here, the characteristic velocity V_0 is given by

$$V_0^2 = \frac{F_0 d}{4\phi\rho R\,(R^2 - R_0^2)}. \tag{8}$$

Indeed, data in fig. 3(a) collapse on to a single master curve representing eq. (7) in fig. 4, justifying the nontrivial assumption. Here, the numerical constant k can be estimated as 0.638, of the order of unity as expected.

It is possible that the size of the percolated cluster depends not only on M but also on ϕ. This means the coefficient k can be a function of ϕ. This point is now under study.

Image analysis of the percolated cluster. To justify further the above picture of percolated cluster we performed a series of image analysis. We visualize the region where dynamical force chains are connected with the granular particles within the first shell around the obstacle in the following way. Here, the thickness of the first shell is defined as the diameter of particles, $2d$. We created a binary (black and white) image by subtracting two snapshots separated by the time during which the cell moves by the distance $2d$ (in the frame fixed to the desk). As a result, the regions in which the particles move and do not move become black and white, respectively. The size of the black region thus visualized gives a measure of the percolated cluster.

A typical example of the binary image is shown in fig. 5(a). From the black area πR_c^2 we estimate an effective radius R_c of the cluster. The radius of the largest circle in fig. 5(a) corresponds to R_c in this case. Although the shape and size of the black area fluctuate significantly as the bare forces in fig. 2, the average (of 30 such binary images for a fixed drag velocity) is again well defined. Such an average radius R_c is plotted in fig. 5(b) as a function of the obstacle (outer) radius R for a fixed drag velocity $V = 100\,\mathrm{mm/s}$. This demonstrates that the cluster size scales as the obstacle size. The slope of the dashed

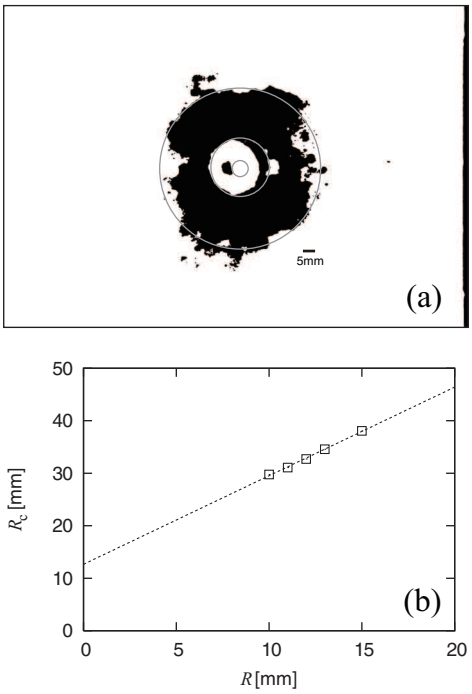

Fig. 5: (a) A binary image suggesting the size of the percolated cluster by a black region. The two smaller circles indicate the size of the washer (obstacle). The largest circle stands for the size of the cluster estimated from the black area. The thickness of the black vertical bar on the right corresponds to the first-shell thickness, $2d$. (b) The average size R_c of the percolated cluster as a function of the obstacle size R.

line fitting the data is 1.69, of the order of the unity, as expected. This analysis predict that the factor $m/(m+M)$ in eq. (6) is nearly a constant about 0.7.

The fitting line intersects with the vertical axis around at $R_c = 10\,\mathrm{mm}$. This indicates that when the size of the obstacle become of the same order of granular particles there still remains a strong velocity correlation within a distance of several times of particles around the obstacle. This indication is consistent with the previous studies on velocity correlations in granular media which do not contain larger obstacles (see, *e.g.*, [22]).

Discussion. –

Comparison with previous studies. A direct study on drag friction at a constant speed in a two-dimensional geometry [14] reported no velocity dependence of the drag force in a velocity region similar to our experiment. However, in this experiment the intruder was fixed at depth of 500 mm; the experiment was performed under a strong influence of gravity. As a result the drag friction was understood by a Coulombic friction saturated to the Janssen's value [23,24], which is independent of velocity. On the contrary, the gravity effect is completely removed in our experiment so that the drag force in our experiment must have a different physical origin; the different velocity-dependence in [14] is not surprising but natural.

The squared-velocity dependence of the drag force has been discussed in simulations on dilute granular media [15–17] and also in impact experiments [12,13]. However, if we compare the squared velocity term in these previous studies and that in the present study, we find that their physical origins are rather different. In the previous studies, this term has been understood as a hydrodynamic inertial force of granular medium. Accordingly, the proportional coefficient scales as cross-sectional area. In three-dimensional (3D) cases this implies a force term $\rho' R^2 V^2$ (with R the size of a spherical obstacle) as indicated in impact experiments [12,13]. This inertial friction in the present two-dimensional (2D) case implies a force term $\rho' R d V^2$ as implied in [15–17]. This is different from the non-hydrodynamic force proposed in eq. (7), which essentially scales as $\rho(R^3/d)V^2$ in 2D (and $\rho(R^5/d^3)V^2$ in 3D). As a matter of fact, the order of magnitude of the hydrodynamic friction $\rho' R d V^2$ is too small to explain our experimental results; the hydrodynamic and non-hydrodynamic frictions can be easily distinguished experimentally because the difference (or ratio) of the order of $(R/d)^2\rho/\rho'$ is large enough. Furthermore, we confirmed that the data cannot be collapsed via the hydrodynamic friction. Our friction is non-hydrodynamic as demonstrated in fig. 4.

The hydrodynamic friction is expected when collision is essentially binary. Indeed, this can be confirmed from eq. (2) because the factor $m/(m+M)$ in eq. (6) is replaced by m/M for binary collision. In the dilute limit or in the short collision time limit, this binary assumption should be almost exact. Accordingly previous results have been explained well by the hydrodynamic friction. Note that in the impact experiments, compared with ours, the granular size is much smaller and the velocity range is much larger. Both factors tend to reduce the collision time, almost validating the binary assumption. However, when the collision time becomes longer we expect the granular nature of the medium is enhanced and the dynamical force chains formed on the time scale of collision come into play a significant role in the drag friction. The present results imply that there is a regime in which these chains percolated in the whole fluidized region. In such a non-hydrodynamic case, the momentum transfer per collision becomes larger, compared with the binary or hydrodynamic case. This is the reason why the order of magnitude of the friction in our case is much larger compared with the hydrodynamic friction but our friction still scales as squared velocity.

Other possible contributions to friction force. We confirmed that the friction between the disk-obstacle surfaces and cell plate and that between the thread and the cell are negligible compared with the typical drag force in question. This is confirmed by comparing drag forces with and without small particles. The latter force is negligible to the former.

The other possible unwanted friction is the friction between particles and top cover or the bottom plate of the cell. To experimentally confirm that this friction is low, we also did experiments with covering the surface of the cell plate with a Teflon sheet. This significantly changes the friction coefficient of the plate. However, we find no difference in the obtained data to confirm the low friction.

The reason of this low friction is understood as follows. We use light sphere particles instead of cylindrical disks used, *e.g.*, in [11,25]. Sphere balls contacts with plates only by a point (while disks by a plane). In addition, the force acting on the contact point is weak because particles have light weight and the cell depth is slightly larger than particle diameter $2d$. As a result the balls are very easy to roll on the plate causing only little friction with the plates.

Due to this low friction, we can put a lid to avoid particles pop out from the cell in the high-velocity region of interest. This implies small movements in the direction perpendicular to the cell plane although severely restricted. However, we can neglect this in the present context. This is because our theory is based on momentum change in the drag force direction and the movement in this direction is independent of that in the direction perpendicular to the cell plane. This is guaranteed by the low friction between particles and plates.

Importance of homogeneity in polydispersity. As explained below we can fix the homogeneity in polydispersity of balls along the trail of the percolated cluster during multiple drags. This homogeneity is very important for reproducibility. Indeed, although ϕ is fixed in this study, if we change (homogeneous) polydispersity the force-velocity curves are shifted (*e.g.*, compare R10a and R10b in fig. 3(a)). However, when renormalized using F_0 all the data collapse on to the same curve, as seen in fig. 4.

Way of fixing (homogeneous) polydispersity. We can fix (homogeneous) polydispersity on the trail by performing a set of multiple-ten-drag experiment for a given R and for various V without opening the top cover. This is because the segregation after multiple ten drags is negligible. We pull manually the resetting line (see fig. 1(a)) to the left to move the obstacle back to the original position and gently tap the cell for homogenization, before starting a new drag. This procedure guarantees the reproducibility of the data, indicating that the (homogeneous) polydispersity is fixed well on the trail. However, the polydispersity generally changes once we open the top cover and refill the contents even if ϕ is fixed; in such a case the reproducibility is no longer guaranteed.

Slow-velocity regime. Our present study concentrates on a high-velocity region; eq. (7) does not capture the full velocity dependence. As a matter of fact, at velocities smaller than 100 mm/s the force-velocity data points deviate off below the curve extrapolated from the curve in the larger velocity region (not shown in fig. 3). In addition, this granular medium always exhibits a finite yield stress

at $V = 0$ whose value is roughly half of F_0. We have yet to study in detail the small velocity region, including dependence of F_0 and of the yield stress on volume fraction or on polydispersity.

Conclusion. – We have demonstrated that an average drag force on an obstacle in a 2D granular system follows eq. (7) through a distinct data collapse with an aid of simple but nontrivial arguments. The arguments give an insight into the granular nature of the friction. A moving obstacle creates a fluidized region around itself causing a dynamical phase separation. Inside the fluidized region dynamical force chains are developed on the time scale of collision. Due to the force chains collision to a single small particle (*i.e.*, binary collision) is difficult to happen. Rather, the obstacle collides with a percolated cluster connected by the force chains at each collision. This non-hydrodynamic nature reflecting the existence of force chains predicts a drag force scaling as $\rho(R^3/d)V^2$ in the present 2D case (and $\rho(R^5/d^3)V^2$ in 3D), different from the inertial force ($\rho' RdV^2$ in 2D and $\rho' R^2V^2$ in 3D) implied in the previous studies. It is this non-hydrodynamic force that explains our experimental results quite well. The drag force transition from the hydrodynamic to non-hydrodynamic squared-velocity dependent friction should be an important future problem for fundamental understanding of the granular dynamics.

* * *

KO thanks MEXT, Japan for KAKENHI. We thank Hiroaki Katsuragi for useful comments.

REFERENCES

[1] Duran J., *Sables émouvants: La physique du sable au quotidien* (Berlin, Paris) 2003.
[2] Jaeger H. M., Nagel S. R. and Bheringer R. P., *Rev. Mod. Phys.*, **68** (1996) 1259.
[3] De Gennes P. G., *Rev. Mod. Phys.*, **71** (1999) S374.
[4] Forterre Y. and Pouliquen O., *Annu. Rev. Fluid. Mech.*, **40** (2008) 1.
[5] Johnson P. A. and Jia X., *Nature*, **437** (2005) 871.
[6] Liu A. J. and Nagel S. R., *Nature*, **396** (1998) 21.
[7] Drocco J. A., Hastings M. B., Reichhardt C. J. O. and Reichhardt C., *Phys. Rev. Lett.*, **95** (2005) 088001.
[8] Wieghardt K., *Annu. Rev. Fluid. Mech.*, **7** (1975) 89.
[9] Albert R., Pfeifer M. A., Barabási A. L. and Schiffer P., *Phys. Rev. Lett.*, **82** (1999) 205.
[10] Hartley R. R. and Behringer R. P., *Nature*, **421** (2003) 928.
[11] Candelier R. and Dauchot O., *Phys. Rev. Lett.*, **103** (2009) 128001.
[12] Katsuragi H. and Durian D. J., *Nat. Phys.*, **3** (2007) 420.
[13] Goldman D. I. and Umbanhowar P., *Phys. Rev. E*, **77** (2008) 021308.
[14] Chehata D., Zenit R. and Wassgren C. R., *Phys. Fluids*, **15** (2003) 1622.
[15] Buchholtz V. and Pöschel T., *Granular Matter*, **1** (1998) 33.
[16] Zenit R. and Karion A., *Granular flow around a cylinder,* in *Proceedings of the 2000 AIChE Annual Fall Meeting, Los Angeles, CA, 2000.*
[17] Wassgren C. R., Cordova J. A., Zenit R. and Karion A., *Phys. Fluids*, **15** (2003) 3318; Bharadwaj R., Wassgren C. and Zenit R., *Phys. Fluids*, **18** (2006) 043301.
[18] Bagnold R. A., *Proc. R. Soc. London, Ser. A*, **225** (1954) 49.
[19] Mitarai N. and Nakanishi H., *Phys. Rev. Lett.*, **94** (2005) 128001.
[20] Eri A. and OKumura K., *Phys. Rev. E*, **76** (2007) 060601(R); **82** (2010) 030601(R).
[21] Brilliantov N. V. and Pöshel T., *Kinetic Theory of Granular Gases* (Oxford University Press) 2004.
[22] Pouliquen O., *Phys. Rev. Lett.*, **93** (2004) 248001.
[23] Janssen H. A., *Z. Vereins Dtsch. Ing.*, **39** (1895) 1045.
[24] Duran J., *Sables Poudres et Grains* (Eyrolles, Paris) 1997.
[25] Kolb E., Cviklinski J., Lanuza J., Claudin P. and Clément E., *Phys. Rev. E*, **69** (2004) 031306.